24th INTERNATIONAL CONGRESS ON SOUND AND VIBRATION
23–27 July 2017, London

ICSV24
23-27JULY 2017
LONDON CALLING

NUMERICAL PREDICTION OF CABIN NOISE DUE TO JET NOISE EXCITATION OF TWO DIFFERENT ENGINE CONFIGURATIONS

Christopher Blech and Sabine C. Langer
TU Braunschweig – Institute for Engineering Design, 38106 Braunschweig, Germany
email: c.blech@tu-braunschweig.de

Christina K. Appel and Jan W. Delfs
German Aerospace Center – Institute of Aerodynamics and Flow Technology, 38108 Braunschweig, Germany
email: christina.appel@dlr.de

The development of environmental friendly aircraft requires, inter alia, a drastic reduction of aircraft noise. In the framework of the Collaborative Research Centre (CRC) 880, an aircraft with innovative high-lift systems is investigated. In comparison to a conventional engine on under-wing position, an Ultra High Bypass Ratio (UHBR) engine on over-wing position is expected to reduce the sound radiation towards the ground. To ensure the acceptance of this configuration, a potential negative impact on the cabin noise must be excluded. As the UHBR engine is installed closer to the passenger cabin and as the engine generates sound at lower frequencies due to its larger dimensions, a more effective sound transmission into the cabin is expected. Apart from that, less sound is radiated due to a reduced rotational speed of the UHBR engine. In this contribution, the hybrid computational aeroacoustic (CAA) solver PIANO combined with the FRPM method is applied to compute the pressure fluctuations due to jet noise on the outer surface of the fuselage. This approach uses the turbulence statistics from an underlying RANS computation to model the fluctuating sound sources and involves the mean flow data for the sound propagation. In a second step, the pressure fluctuations are applied to a generic mechanical model of the fuselage which is solved in frequency domain by the in-house code ELPASO using the Finite Elements Method (FEM). The model includes the double wall structure, insulating material and the enclosed fluid cavities. The approach results in the differences of the cabin's mean pressure of both engine configurations.

1. Introduction

In acoustics, a task in early design stages is the comparison of engine configurations with regards to cabin noise. In the design of quiet aircraft, an UHBR engine on over-wing position is a promising alternative to a conventional engine. To exclude a potential negative impact of the UHBR engine on the cabin noise, the entire chain of modelling the background flow, airborne sound paths, structure-borne sound paths within a pre-designed aircraft structure and the cabin fluid itself must be addressed. As a first step, a methodology for giving an assessment of cabin noise due to jet noise is presented. The following sections describe a two-step approach first implemented in this contribution. By means of CAA calculations (Section 3), pressure fluctuations for an UHBR and a conventional CFM-56 engine are calculated on the basis of mean flow data and statistical turbulence quantities (Section 2). Both loads are applied on a generic model of the coupled aircraft's structure and fluid domain (Section 4). The mean pressure within the cabin can directly be compared as basis of the assessment (Section 5).

2. RANS computation of underlying flow

The applied computational approach is a hybrid method for broadband jet noise prediction (Ewert et al. [7, 14, 15]). It includes the following steps: A RANS computation, which provides mean flow data and statistical turbulence quantities, modelling of fluctuating sound sources derived from the Tam & Auriault [19] (T&A) cross-correlation model and a CAA prediction step using the previously computed fluctuating sound sources.

In the current case a very well resolved boundary layer at the fuselage is needed. Therefore, the generic aircraft fuselage is computed isolated. In addition, an isolated RANS meanflow of the jet flow has to be computed. By separating both parts, the geometry is kept very simple so that the hexahedral mesh part at the fuselage surface is not limited regarding the total height due to wing fuselage transition. The isolated engine allows to employ an axis-symmetric grid for the jet flow.

The RANS computations have been performed with the DLR flow solver TAU (version 2015.2). It is an unstructured solver, which can also handle structured grids, once converted to an unstructured grid format. The advantages of structured meshes for aligned flows like boundary layer or jet flows can be kept. The isolated fuselage is meshed with a quad-dominated SOLAR mesh. The boundary layer is resolved with 45 grid points in wall normal direction within the structured part. In total, the fuselage mesh has about 1.85 mio. points. The turbulence modelling is done by means of the RSM-g turbulence model [20] (Reynolds Stress model). The environment conditions are according to cruise conditions, as described in the CRC reference configuration [17].

The axis-symmetric jet flow is computed isolated with a 15 degree, structured mesh segment. Symmetry conditions were applied at the boundaries. The mesh consists of a 2D grid, which was revolved up to the desired angle. The mesh extent is 15D in radial and 30D from the engine outlet in axial direction. Turbulence modelling is done by means of the Menter-BSL (Baseline) turbulence model [13]. The geometry of the conventional engine is based on a CFM-56 engine, which is adapted in its dimensions according to the design introduced by the CRC transport aircraft reference configuration [17]. The thermodynamic cycle data was provided by the software GasTurb of the Institute of Jet propulsion and Turbomachinery of Technische Universität Braunschweig. The design of the UHBR engine was prepared as part in a diploma thesis [12] by means of the codes PrADO [21], GasTurb and the Noise prediction tool PANAM [3]. The diameters of the UHBR and the conventional engine bypass duct are 1.78 m and 1.568 m respectively. Both designs are depicted in Fig. 1 right. The meshes for the engines are prepared with the Gridgen/Pointwise mesh generator and are resolved with about 200,000 grid points per radial-axial plane and 19 points in azimuthal direction.

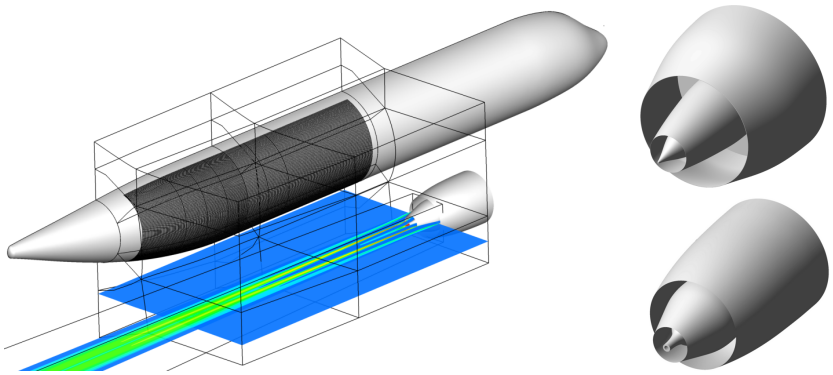

Figure 1: Computational CAA domain for the conventional engine, illustrated with the distribution of the TKE. The black dots indicate the sampling positions at the fuselage surface (left). Nozzle geometries: UHBR (top, right) and conventional (bottom, right).

3. CAA model of fluctuating sound sources

The next step is to derive the acoustical sources of the jet mixing noise from the Tam & Auriault [19] cross-correlation model and realised in the fast Random Particle Mesh method (F)RPM [5, 6] as a scalar quantity, which shows up at the right hand side of the pressure equation of the linearised Euler equations.

A set of minimum two meshes is needed: The CAA mesh, which extends to the needed computational domain and a rectangular 3D FRPM background mesh with equidistant grid points, where the acoustic sources corresponding to the chosen source term are generated. If the source domain, as in the current case, is quite huge, it is possible to speed up by using several background meshes, overlapping each other, as it was also done in e.g. Neifeld et al. [16]. To avoid additional sources, there has to be a carefully adjusted blending in between the overlapping grid patches.

In the formulation for (F)RPM/PIANO, the stochastically realised sources q_p appear on the RHS of the pressure equation of the linearised Euler equation (LEE):

$$\rho_0 \left[\frac{\partial u'}{\partial t} + u_0 \nabla u' \right] + \nabla p = 0 \frac{\partial p}{\partial t} + u_0 \nabla p + \gamma p_0 \nabla \cdot u' = q_p \tag{1}$$

In the present study, the fluctuating sources are provided by the jet mixing noise sources, which are derived from the T&A two-point space-time correlation model.

$$q_p \equiv \frac{Dq_s}{Dt} \tag{2}$$

$$\left\langle \left(\frac{Dq_s}{Dt} \right)_1 \left(\frac{Dq_s}{Dt} \right)_2 \right\rangle = \frac{\hat{q}_s^2}{c^2 \tau_s^2} \times \exp \left\{ -\frac{|\xi|}{u_{jet} \tau_s} - \frac{ln2}{l_s^2} [(\xi - u_j \tau)^2 + \eta^2 + \zeta^2] \right\}. \tag{3}$$

In this equation, ξ, η and ζ are the space separations between two correlated points and τ is the time delay. l_s is the length scale, τ_s is the time scale and the term in front of the exponential function is the source variance, where $\hat{q}_s^2$ is the RMS value of the fluctuating kinetic energy. c is a time scale coefficient, which controls the turbulence decay time according to the fluctuating time of the source correlations.

The stochastical realisation of Eq. (3) in (F)RPM is

$$\frac{Dq_s(x,t)}{Dt} = \int_{V_S^n} \hat{A}(x) G\left(|x - x'|, l_s\right) \mathcal{U}\left(x', t\right) \mathrm{d}^n x'. \tag{4}$$

Here, $\hat{A}$ is the source variance, G is a Gaussian filter kernel to provide a spatial filtering of each particle and $\mathcal{U}$ represents spatio-temporal white noise. The index n denotes the dimension of the problem. In detail the PIANO/FRPM for jet noise method introduced in e.g. Neifeld et al. [16].

Fig. 1 left shows the computational domain for the conventional configuration. Originally, the CAA mesh consists out of 16 blocks with about 72 mio. points. For parallelisation purposes, the blocks have been split into 945 smaller blocks. The maximal resolved frequency of the CAA mesh is 2 kHz. According to this point sampling positions at the fuselage surface are defined, which allow an appropriate spatial resolution. In total ca. 83000 sampling points are specified for the conventional configuration. The UHBR configuration gets along with 53000 positions due to the smaller extend of the CAA mesh. The computation time for the conventional case was 7 days@216cpus.

Fig. 2 illustrates the instantaneous pressure at the fuselage (left: conventional, right: UHBR). Qualitatively, the levels for the UHBR are lower, as expected due to the lower jet velocity. But the spatial structures on the UHBR plot indicate much higher frequencies, what seems not realistic, if one consider just the larger dimensions of the engine. Furthermore, a comparison with calculations with the 2.5D tool PIANO/RPM modal [14] (not shown here), suggests that the application of the T&A jet mixing noise model as it was implemented in PIANO/FRPM e.g. Neifeld et al. [16] is not

correct here. So the effect of additional co-flow, what can be captured in the original T&A Model, can not be reproduced correctly with FRPM. The used CAA data show up shortcomings, but these shortcomings are consistent for both configurations, hence a comparison with each other is acceptable. Nevertheless, the work on these issues is continued.

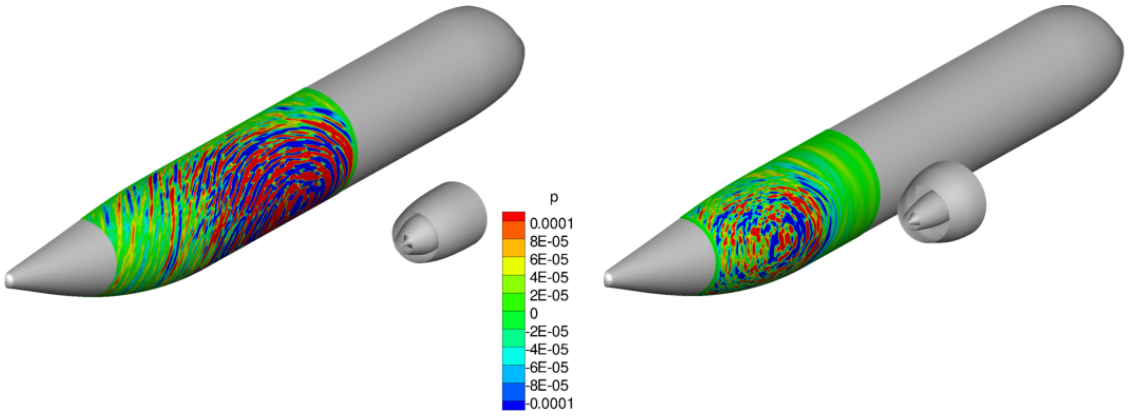

Figure 2: Instantaneous pressure fluctuations on the fuselage surface: conventional nozzle (left) and UHBR (right).

4. Generic mechanical model of the aircraft's fuselage

The calculated excitations by the conventional and the UHBR engine configuration are both applied to one identical mechanical model of the aircraft's fuselage [1, 2]. Due to the fact of roughly given information on the aircraft's dimension in the early design stage and a focus on the methodology in this contribution, a generic model is applied here. Systematic modelling errors would still allow a comparison of the induced cabin noise, but the results are limited to the comparison and cannot be interpreted as absolute quantification. The model is formulated in frequency domain; general assumption are:

1. stationary response in cruise flight
2. symmetric problem with inversely phased excitation by the two identical engines in cruise flight
3. neglected influence of the aircraft's structural front partition (cockpit to wing box)

The latter is justified with the jet noise excitation affecting only the rear part of the aircraft and the wing box bringing a reflecting impedance jump into the system. An overview of the mechanical model used for the computation is shown in Fig. 3. The model considers the primary structure (green), the secondary structure (yellow), the cabin fluid cavity (light blue) and the insulation (dark blue) between the primary and secondary structure. In the figure, the cabin fluid part is cut for visualisation due to its length of 17 m.

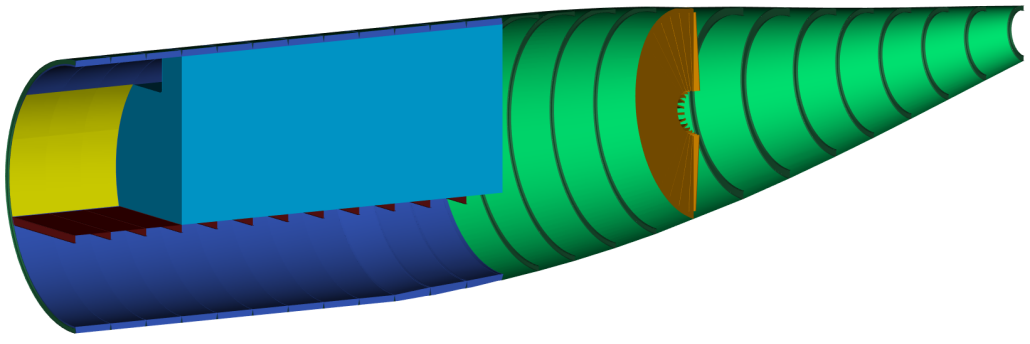

Figure 3: Mechanical model applied for the prediction of cabin noise (entire cabin not shown)

The primary structure of the aircraft is mechanically modelled by a classical shell formulation, combining structural disc and plate (Reissner-Mindlin) formulations [4]. Hence, in-plane waves and bending waves are represented which is reasonable for the complex cylindrical structure. All parts of the primary structure, the thin cylinder (green), the the bulk head (orange) and the cylindrical frames (dark green) are modelled as shell structure. As no dimension is given for the length-wise stringers in the current early design stage, they are neglected for the comparison of the two engines. The material of the cylindrical shell and the frames is a ten layer carbon-fibre-reinforced plastic (CFRP) which is modelled as visco-orthotropic material using engineering constants for the real part of the young's modulus. The shell's thickness h varies as a result of an optimisation process with several typical load cases [18]. The loss factor is generally assumed as $\eta = 0.01$ for a complex structure with joints, according to [9], see Eq. 5. The floor partition is similarly considered with a variable thickness for its stiffeners (dark red) and a constant thickness for the floor itself (red). Both parts of the floor are made of CFRP and modelled using a visco-orthotropic material model ($\eta = 0.01$):

$$\underline{E}_{x/y} = E_{x/y}(1 + i\eta) \tag{5}$$

The secondary structure, which consists of the cabin linings and the ceiling (yellow), is realised with typical Honeycomb panels made of a Honeycomb and two outer layers of glass-reinforced plastic (GRP). As mechanical representation, the mentioned shell formulation with a visco-elastic material model using engineering constants is applied. Respectively, the linings are ideally fixed to the cylindrical frames at each corner.

The cabin fluid cavity mainly involves the cabin air (blue), the seats and the passengers. For a first assessment, the cavity is modelled as ideal fluid.

The insulation is realised by typical glass wool applied in aircraft (dark blue). The mechanical model considers an equivalent fluid approach [11] with material data taken from [8].

Structural and fluid parts are fully coupled and solved using the Finite Element Method (FEM). The formulation of the structural parts are discretised by 9-node quadrilateral elements and the fluid parts are discretised by 27-node hexaeder elements, both using quadratic ansatzfunctions. A strong coupling is performed [4, 10]. The frequency range is set to $0 - 710\,\text{Hz}$ which requires a certain mesh resolution calculated for the minimum wave length in the thin shells and the wave length in air $\lambda = c/f_{max}$. The structural wave length is analytically approximated by this formula based on [9]:

$$\lambda_{min} = \frac{2\pi}{\sqrt{\omega_{max}}} \sqrt[4]{\frac{B}{\rho h}} \tag{6}$$

B is the bending stiffness and ρ the density. The determined element side edge lengths, the corresponding wave lengths and the resulting number of degrees of freedom (dof) are given in table 1.

Table 1: Mesh sizes realised for the FE discretisation of the mechanical model.

Part	$\lambda(f_{max})$ [m]	h_{Elem} [m]	dof
Thin cylindrical shell & frames (green)	0.122	0.061	707070
Bulk head (orange)	0.173	0.087	52722
Floor & frames (red)	0.160	0.080	64764
Cabin linings & ceiling (yellow)	0.389	0.195	88320
Cabin fluid cavity (blue)	0.483	0.242	299697
Insulation (dark blue)	0.183	0.091	118437
			1331010

A minimum of five nodes per wave length for the most critical part is demanded in the sense of the smallest wave length within the thinnest outer shell at the highest frequency. The corresponding

side edge length also determines the element size of the entire outer structure, the frames and the insulation material as the meshing process realises a regular mesh, see Fig. 4 .

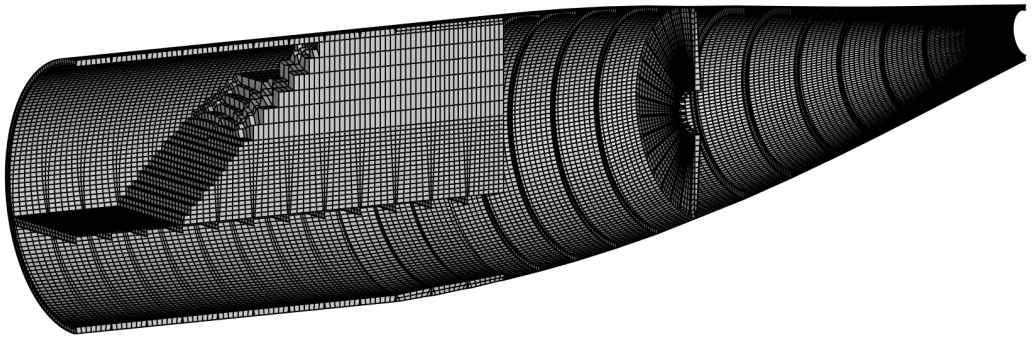

Figure 4: Finite element mesh used for the solution of the mechanical model.

The calculated pressure fluctuations on the outer surface are transformed into frequency domain using a fast fourier transformation (FFT) in MATLAB for each available sampling point. A script reads in the shell elements and interpolates the given data to the mid-side nodes of each affected element of the outer shells. Amplitude and phase is applied as pressure load according to position and frequency.

5. Results

Given the fact that the load data contains a systematic frequency shift (see section 3) and the fluid-structural model is in general applicable for a comparison of configurations, the difference in the mean sound pressure level per third octave band is shown in Fig. 5:

$$\Delta L_p(f) = L_p(f)_{UHBR} - L_p(f)_{KONV} \tag{7}$$

The UHBR engine results in higher sound pressure levels within the cabin. Due to the frequency shift, negative values are expected at higher frequencies, corresponding to a louder conventional engine. The model has to be adopted to be applicable for higher frequencies and the load modelling has to be improved in further studies.

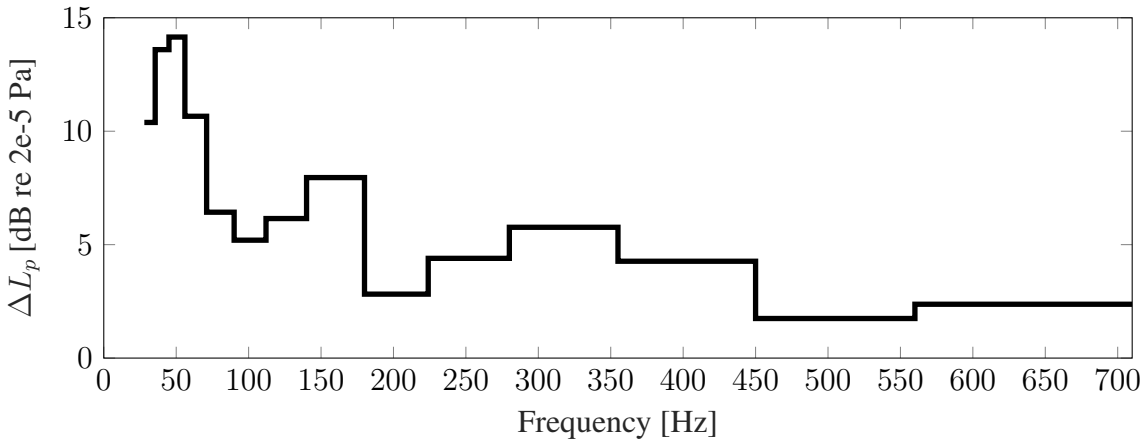

Figure 5: Difference in the mean sound pressure level $\Delta L_p(f)$ between the UHBR and the conventional engine configuration per third octave band.

Additionally, the sound pressure sum level ($0 - 710\,\mathrm{Hz}$) for the UHBR configuration at each position in the cabin (at passenger's ears) is shown in Fig. 6. As expected, maxima can be seen within the edges and in the symmetry plane. The latter is reasonable, as only uneven fluid modes are excited which always have a pressure maximum in the symmetry plane. Furthermore, the sound pressure levels are tending to be higher in the back of the aircraft, which is also expected.

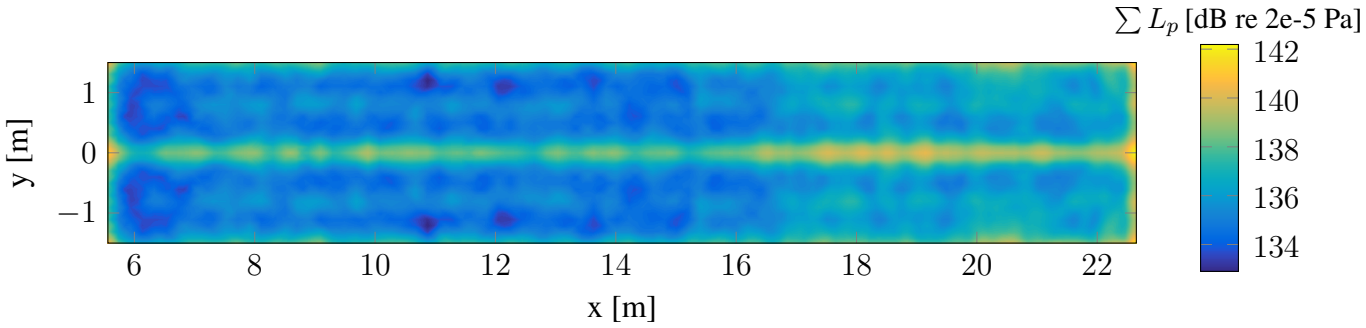

Figure 6: Spatial distribution of the $\sum L_p$ of the UHBR engine configuration.

6. Summary and Outlook

The contribution presents a methodology applicable in early design stages to assess two different engine configurations. The entire modelling chain is shown and systematic deviations in all steps are discussed in particular. As immediate next step, the current applied CAA model is improved to overcome the mentioned discrepancies. Further studies concentrate on more detailed models of the fluid-structural part, mainly considering the full aircraft and higher frequencies which require finer meshes. Furthermore, the influence of length-wise stringers, windows, doors, seats and passengers on the sound level difference is investigated. The long-term aim of the project is to quantify sound pressure levels within the cabin and make them audible.

Acknowledgement

The authors would like to thank the *Sonderforschungsbereich 880* of the *Deutsche Forschungsgemeinschaft* and its graduate research program *Modul Graduiertenkolleg (MGK)* for the financial support.

REFERENCES

1. Beck, S.C.; Langer, S.: *Modeling of flow-induced sound in porous materials*, International Journal for Numerical Methods in Engineering, (2014) Vol. 98 (1), pp 44-58

2. Beck, S.C.; Müller, L; Langer, S.: *Numerical assessment of the vibration control effects of porous liners on an over-the-wing propeller configuration*, CEAS Aeronautical Journal, (2016) Vol. 7(2), pp 275-286

3. Bertsch, E. L.: *Noise Prediction within Conceptual Aircraft Design* Dissertation, TU Braunschweig, 2013

4. Clasen, D.; Langer, S.: *Finite element approach for flanking transmission in building acoustics*, Building Acoustics, (2007) Vol. 14 (1), pp 1-14

5. Ewert, R.: *RPM - the fast Random Particle-Mesh method to realize unsteady turbulent sound sources and velocity fields for CAA applications*, AIAA 2007-3506.

6. Ewert, R.: *Broadband slat noise computations based on CAA and stochastic sound sources from the fast random particle-mesh (RPM) method*, Computer and Fluids, 37(4), 2008.

7. Ewert, R.; Neifeld, A.; Fritzsch, A.: *A 3-D modal stochastic jet noise source model*, AIAA 2011-2887.

8. Gündel, A.; Häusler, S.; Marburg, S.: *Vergleich verschiedener Absorbermodelle zur Berechnung von Flug-innenlärm unter Beachtung poröser Materialien*, Proceedings, DAGA, Stuttgart, 2007.

9. Kollmann, F. G.: *Maschinenakustik: Grundlagen, Meßtechnik, Berechnung, Beeinflussung*, Springer-Verlag, 2011.

10. Langer, S.; Antes, H.: *Analyses of sound transmission through windows by coupled finite and boundary element methods*, Acta Acustica united with Acustica, (2003), Vol. 89 (1), pp 78-85

11. Langer, S.; Al-Kharabsheh D. and Wulkau, M: *On the Sensitiveness of Absorption Coefficient to Changes in Material Parameters.* PAMM 9.1 (2009): 513-514.

12. Lehmler, M.: *Estimation of an ultra high bypass ratio turbofan engine in terms of actual aircraft operation*, Diploma thesis at the IFAS, TU Braunschweig, 2016

13. Menter, F. R.: *Two-equation eddy-viscosity turbulence models for engineering applications*, AIAA J., 32(8),1994.

14. Neifeld, A.; Ewert, R.: *Jet Mixing Noise from Single Stream Jets using Stochastic Source Modeling*, AIAA 2011-2700.

15. Neifeld, A.; Ewert, R.: *On the Contribution of Higher Azimuthal Modes to the Near- and Far-Field of Jet Mixing Noise*, AIAA 2012-2114.

16. Neifeld, A.; Ewert, R.; Keller, D.; Steger, M.: *Towards Prediction of Jet Noise Installation Effect using Stochastic Source Modeling*, AIAA 2014-3059 in Europe: The CEAS-ASC report on 2013 highlights, Contribution, JSV, 340, pp. 39-60.

17. Radespiel, R.; Heinze, W.: *SFB 880: fundamentals of high lift for future commercial aircraft*, CEAS Aeronautical Journal, (2014) Vol. 5, pp 239-251

18. Rieke, J.: *Bewertung von CFK-Strukturen in einem multidisziplinären Entwurfsansatz für Verkehrs-flugzeuge*, PhD thesis, in German institute of aircraft design and lightweight structures, TU Braunschweig, CFF-research report 2013-02, published by Cuvillier Verlag, Göttingen, Germany, ISBN 978-3-95404-368-2, 2013.

19. Tam, C.K.W.; Auriault, L.: *Jet mixing noise from fine-scale turbulence*, AIAA J. Vol. 37(2), 1999.

20. Togiti, V.; Eisfeld, B.: *Assessment of g-Equation Formulation for a Second-Moment Reynolds Stress Turbulence Model* AIAA 2015-2925.

21. Werner-Westphal, C.; Heinze, W.; Horst, P.: *Multidisciplinary integrated preliminary design applied to unconventional aircraft configurations* J. Aircr. 45(2), 2008.